Nuclear dissipation at high excitation energy and angular momenta in reaction forming ^{227}Np

M. Shareef,[1,*] E. Prasad,[1,†] A. Jhingan,[2] N. Saneesh,[2] K. S. Golda,[2] A. M. Vinodkumar,[3] Mohit Kumar,[2] A. Shamlath,[1] P. V. Laveen,[1] A. C. Visakh,[1] M. M. Hosamani,[4] S. K. Duggi,[5] P. Sandya Devi,[5] G. N. Jyothi,[5] A. Tejaswi,[5] P. N. Patil,[4] Jhilam Sadhukhan,[6] P. Sugathan,[2] A. Chatterjee,[2] and Santanu Pal[2]

[1]*Department of Physics, School of Physical Sciences, Central University of Kerala, Kasaragod 671316, India*
[2]*Inter-University Accelerator Centre, Aruna Asaf Ali Marg, New Delhi 110067, India*
[3]*Department of Physics, University of Calicut, Calicut 673635, India*
[4]*Department of Physics, Karnatak University, Dharwad 580003, India*
[5]*Department of Nuclear Physics, Andhra University, Visakhapatnam 530003, India*
[6]*Physics Group, Variable Energy Cyclotron Centre, 1/AF Bidhan Nagar, Kolkata 700064, India*

(Received 5 November 2018; published 22 February 2019)

Neutron multiplicity excitation function has been measured for the ^{30}Si + ^{197}Au reaction populating the ^{227}Np compound nucleus at excitation energies in the range 44.1–78.8 MeV using the National Array of Neutron Detector facility of Inter University Accelerator Centre, New Delhi. Measured pre-scission neutron multiplicity values are analyzed using a statistical model incorporating Krammer's fission width due to the dissipative drag in nuclear fission, shell corrections in fission barrier and level density, collective enhancement of level density, and K-orientation effect. The present work demonstrates that a strong fission hindrance is essential to reproduce the experimental pre-scission neutrons, whereas the temperature dependent dissipation coefficient as observed in a few recent measurements is not required to reproduce the experimental $\nu_{\rm pre}$ data. No substantial effect of collective enhancement of nuclear level density and tilting away effect of compound nucleus spin on neutron emission prior to the scission configuration was observed unlike fission of preactinides.

DOI: 10.1103/PhysRevC.99.024618

I. INTRODUCTION

Nuclear fission is a dramatic phenomenon that involves a subtle interplay of macroscopic and microscopic effects. Microscopic effects such as shell effects and pairing play important roles in low energy fission [1], which becomes less significant at high excitations. On the other hand, fission is also known to be a highly dissipative process [2,3] and dissipative effects become increasingly important at higher excitation energies. Though the onset of dissipation has been reported in measurements using various observables [4–6], the exact nature of dissipation and its dependence on various quantities are still not clear.

Pre-scission neutron multiplicity is one of the most important probes to explore the fission dynamics in heavy ion fusion reactions. Neutrons may be emitted from the compound nucleus (CN) itself during the pre-scission stage and/or from the fission fragments after scission. Nonequilibrated processes such as quasifission [7–9] can also contribute to the total neutron multiplicity in reactions involving heavy nuclei. However, such neutrons emitted from the fission fragments (post-scission neutrons) show strong angular correlations due to the kinematic focusing of the fast moving fission fragments, which serves the basis of their separation from the pre-scission neutrons experimentally.

Theoretically, it is possible to estimate the two components of pre-scission neutron multiplicity, the pre-saddle neutron multiplicity ($\nu_{\rm pre\text{-}sad}$), and the post-saddle neutron multiplicity ($\nu_{\rm post\text{-}sad}$). $\nu_{\rm pre\text{-}sad}$ is the average number of neutrons emitted from the system before reaching the saddle point whereas $\nu_{\rm post\text{-}sad}$ is the average number of neutrons evaporated during the descent from the saddle point to the scission point. Estimation of these components of neutron multiplicity was reported to be necessary for the analysis of mass-energy distribution and angular distribution of fission fragments [10,11]. For heavy fissile systems (actinide nuclei), a major contribution to $\nu_{\rm pre}$ comes from the $\nu_{\rm post\text{-}sad}$. This is due to the fact that the nuclei in this region have smaller fission barrier height and also the saddle and ground state configurations have similar deformation values. Hence major de-excitation occurs in the post-saddle phase of shape evolution. Similarly, it is reported that major enhancement in $\nu_{\rm pre}$ with increasing excitation energy is due to the neutrons emitted from the post-saddle phase of the fission process [10,11].

It was reported long ago that the measured pre-scission neutron multiplicities ($\nu_{\rm pre}$) are significantly higher than the statistical model predictions [12–16] assuming the Bohr-Wheeler formalism of fission. Similar observations have also been made for the pre-scission charged particles [17–19] and giant dipole resonance (GDR) γ multiplicities [20–22]. This excess emission is a clear experimental signature [23,24] of dissipation in fusion-fission. Dissipation slows down fission and enhances the particle evaporation probability during the transition of the CN from equilibrium configuration to the scission configuration.

*shareef.m.cuk@gmail.com
†Corresponding author: prasad.e.nair@gmail.com

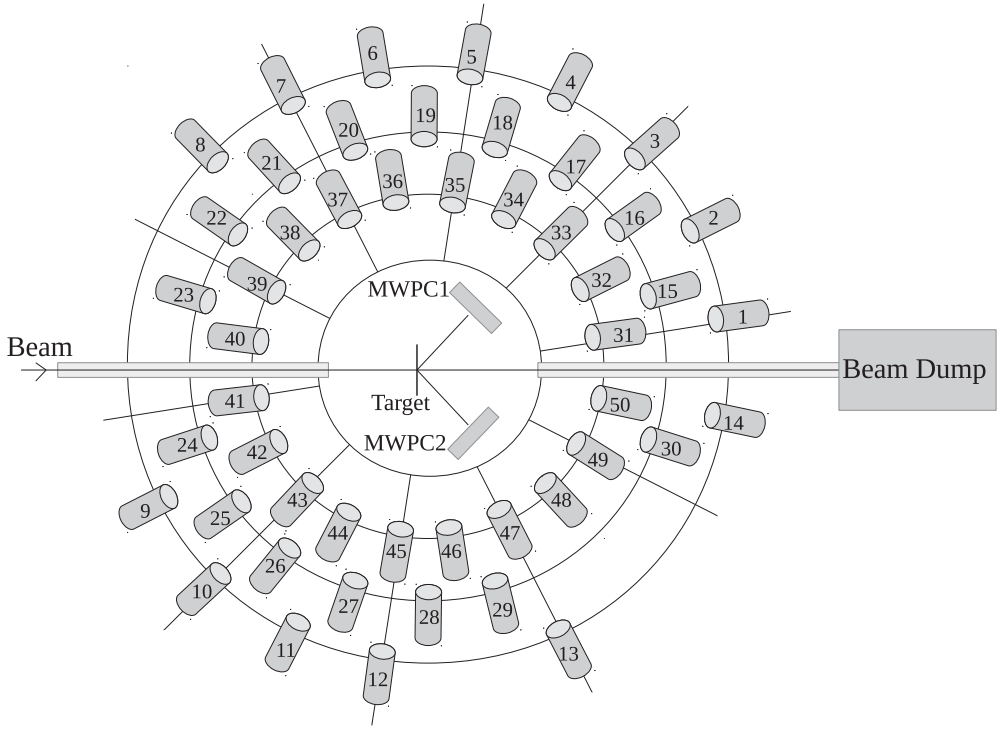

FIG. 1. Schematic of the detector setup of NAND array used in the present study. The neutron detectors are earmarked to indicate their position in the array specified by their respective polar azimuthal angles. See Table I for details.

The dissipation strength in fission dynamics is usually extracted as a fitting parameter in statistical model calculations to reproduce the experimental data. In earlier studies, the dissipation has been found to have a strong excitation energy dependence [4,5,25]. It has further been shown that the excitation energy dependence of dissipation can be attributed to a shape dependence of the dissipation coefficient [25]. It has been suggested that dissipation in fission should have a shape dependence, a smaller value in the pre-saddle region and a higher value in the saddle-to-scission region [26,27]. A recent study also showed that a small dissipation (compared to full one-body dissipation) reproduces the evaporation residue (ER) cross sections, a process essentially determined in the pre-saddle region [28]. On the other hand, multiplicity of pre-scission neutrons emitted by a highly fissile CN would be a suitable tool to study post-saddle dynamics of fission. This is one of the objectives of the present work.

Apart from the effect of dissipation, a recent study of fusion-fission reaction incorporated shell effects, collective enhancement of level density (CELD), and K-orientation effects, in the fission width to model fission. It is shown that the inclusion of these effects provides a consistent picture of fission in the preactinide region [28]. It is, however, reported that CELD is not necessary to reproduce the ER excitation functions of the $^{16}O + ^{208}Pb$ system [29], while the CELD is essential in ^{45}Sc induced reactions on lanthanide targets [30]. In this work, we address the role of CELD in the fission of a highly fissile actinide nuclei populated at high excitation energies. With these motivations, neutron multiplicity measurements have been carried out for the $^{30}Si + ^{197}Au$ reaction leading to the formation of ^{227}Np in this work, at an excitation energy as high as 79 MeV.

The paper is organized as follows. The experimental details are discussed in Sec. II. The data analysis methods and the obtained results are discussed in detail in Sec. III, followed by the theoretical calculations in Sec. IV. Section V presents a general discussion on the finding of this work and the article is summarized in Sec. VI.

II. EXPERIMENTAL DETAILS

The experiment was performed using the 15 UD Pelletron accelerator facility of the Inter University Accelerator Centre (IUAC), New Delhi. Pulsed beams of ^{30}Si from the Pelletron accelerator were further boosted in energy using the superconducting linear accelerator, with a pulse separation of 250 ns used in the experiment to bombard self-supporting, isotopically enriched ^{197}Au target of thickness 300 $\mu g/cm^2$. Measurements were performed at the laboratory energies of E_{lab} = 152.3, 159.4, 166.4, 173.4, 179.4, 186.4 and 192.4 MeV corresponding to the excitation energy range between 44 and 79 MeV.

The schematic of the experimental setup used in the present study is shown in Fig. 1. The target was mounted normal to the beam direction at the center of a spherical scattering chamber of 4 mm thickness and 100 cm diameter. Two silicon surface barrier detectors were placed at $\pm 12.5^\circ$ with respect to the beam direction, inside the scattering chamber, to detect the elastically scattered beam particles. The Rutherford events registered by these monitor detectors were used for beam flux

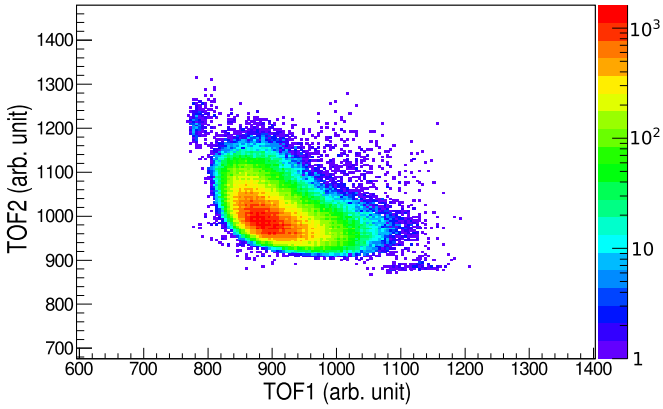

FIG. 2. Time correlation spectra of complementary fragments detected in the MWPC's kept at folding angle direction.

monitoring as well as positioning the beam at the center of the target. The complimentary fission/fission like fragments were detected using a pair of identical position-sensitive multiwire proportional counters (MWPCs). These MWPC's were mounted at $\pm 69^{\circ}$ with respect to beam direction on either side such that the detectors were capable of detecting the complimentary fission fragments. Both detectors have active areas of 11×16 cm^2 and were operated with isobutane gas of 3.5 mbar gas pressure. Time of flight (TOF) spectrum generated from the fast timing signal of the two MWPCs was used for the clean separation of the fission fragments from other possible contaminations. Figure 2 shows two-dimensional correlated TOF spectra from the two MWPCs at 173.4 MeV beam energy.

The neutrons emitted from the CN and fission fragments were detected in coincidence with the binary fission fragments using 50 organic liquid scintillator detectors (BC 501) of the National Array of Neutron Detectors (NAND) facility [31]. These detectors were placed at different polar (θ) and azimuthal (ϕ) angles with respect to the beam direction, as given in Table I. The γ background was suppressed using a beam dump made up of paraffin and lead bricks kept at 4 m from the target position.

Intrinsic efficiency of the neutron detectors used in the experiment were measured using a ^{252}Cf source mounted at the target position. The energy-dependent efficiency of the neutron detectors were obtained by comparing the experimental and theoretical neutron energy spectra for the ^{252}Cf source. Discrimination between the neutrons and γ were achieved using the pulse shape discrimination (PSD) method based on the zero-crossover technique as well as the TOF method [32]. Typical TOF versus PSD spectra from one of the neutron detectors at 173.4 MeV beam energy is shown in Fig. 3.

Versa module europa (VME) based data acquisition system was used for the data collection in the present study. The data were collected event by event and were later analyzed using the software LAMPS [33]. The logical OR of the two fission fragments AND-ed with the radiofrequency signal formed the trigger for the data acquisition system. This logical signal acts as the master start of the TDC as well as the master gate for all ADCs used in the measurement.

TABLE I. Polar (θ) and azimuthal angle (ϕ) of neutron detectors used in the experiment.

Detector No.	θ	ϕ	Detector No.	θ	ϕ
1	18.0	296.5	26	126.1	180
2	31.7	328.3	27	108.1	180
3	47.0	339.9	28	90.0	180
4	63.7	343.7	29	72.0	180
5	80.7	343.7	30	18.0	180
6	99.4	343.7	31	17.2	58.3
7	116.3	343.7	32	30.2	30.0
8	133.0	339.9	33	46.5	22.4
9	149.9	210.0	34	64.9	17.8
10	133.6	202.4	35	81.6	14.7
11	115.2	197.8	36	98.5	14.7
12	98.5	194.7	37	115.2	17.8
13	81.6	194.7	38	133.6	22.4
14	17.2	238.3	39	149.9	30.0
15	18.0	0	40	162.9	58.3
16	36.0	0	41	162.1	116.5
17	54.0	0	42	148.4	148.3
18	72.0	0	43	133.0	159.9
19	90.0	0	44	116.3	163.7
20	108.1	0	45	99.4	163.7
21	126.1	0	46	80.7	163.7
22	144.1	0	47	63.7	163.7
23	162.1	0	48	47.0	159.9
24	162.1	180	49	31.7	148.3
25	144.1	180	50	18.0	116.5

III. DATA ANALYSIS AND RESULTS

The measured neutron TOF spectra were converted into neutron energy spectra using the relation

$$E_n = \frac{1}{2} m_n \frac{d^2}{t^2}, \tag{1}$$

where m_n is the neutron mass, d is the distance between target center and neutron detector, and t is the neutron TOF. The measured neutron spectra consist of the pre-scission neutrons

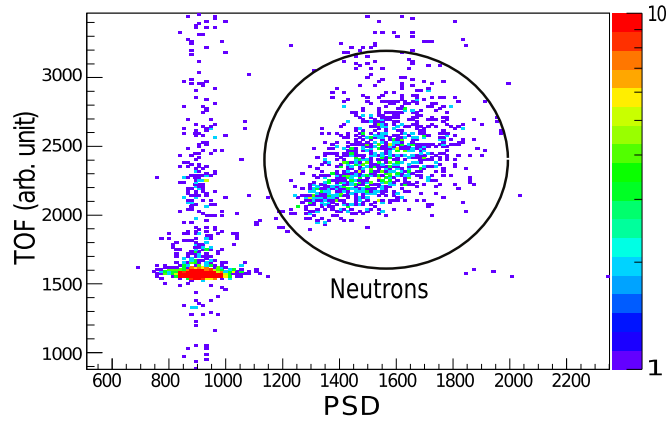

FIG. 3. Pulse shape discrimination (PSD) versus time of flight (TOF) spectra of one of the neutron detectors at 173.4 MeV beam energy.

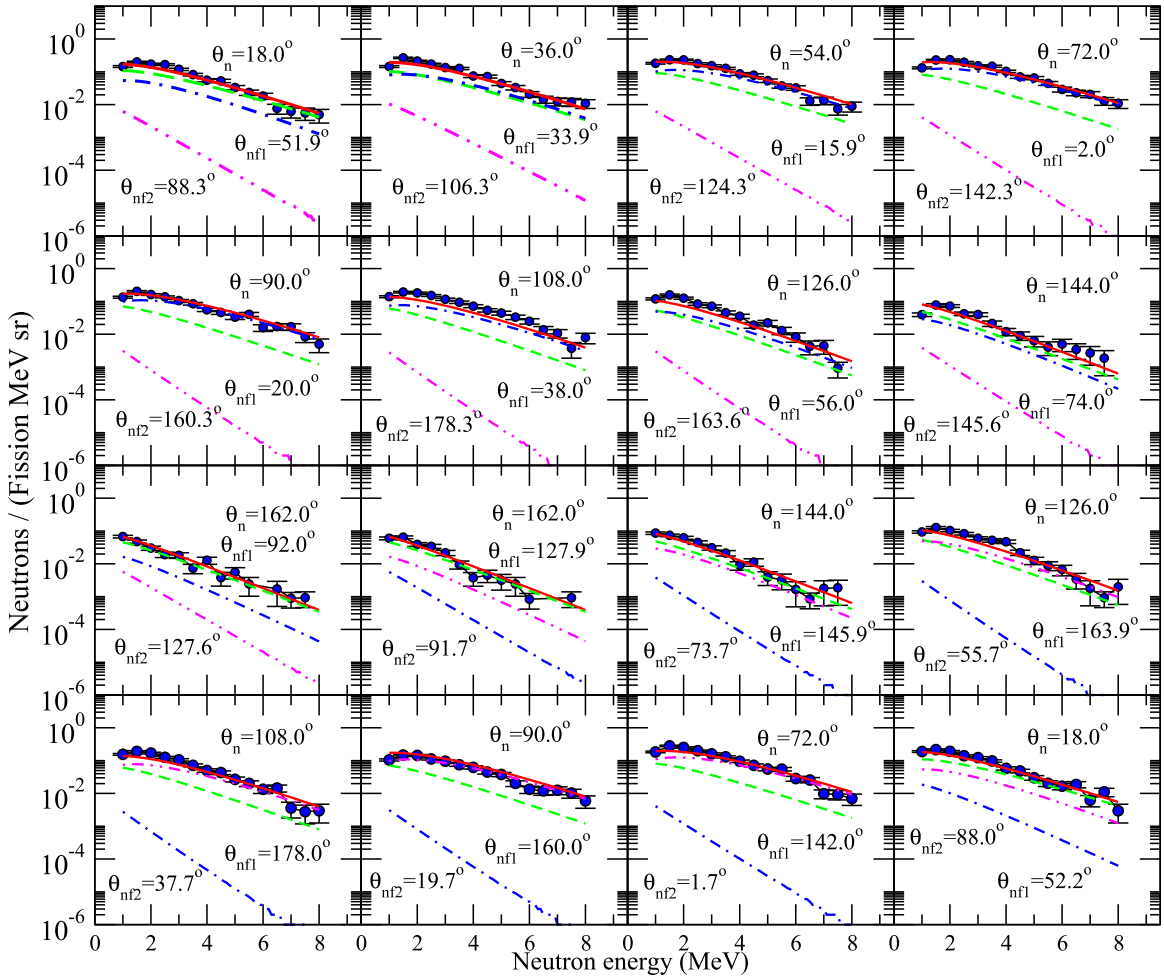

FIG. 4. Experimental double differential neutron multiplicity spectra (solid circles) from ^{227}Np CN at an excitation energy of 62.4 MeV for 16 neutron detectors in the reaction plane. The multiple moving source fits for the pre-scission (dashed lines) and post-scission contribution from one fragment (dotted-dash lines) and that from the other (dotted-dotted-dash lines) are also shown. The total contribution from all the three sources are indicated by the solid line.

emitted from the CN before fission and the post-scission neutrons, emitted from the fast moving fission fragments. The measured neutron energy spectra were thus decomposed into three components, using the moving source model [34]. Neutron emission is assumed be isotropic from three sources in their rest frames in this model. The pre-scission and post-scission neutron multiplicities and temperatures were thus obtained from the experimental neutron energy spectra, using the multiple source fitting of Watt expression [34], given by

$$\frac{d^2M}{dE_n d\Omega_n} = \sum_{i=1}^{3} \frac{\nu_i\sqrt{E_n}}{2(\pi T_i)^{3/2}} \times \exp\left[-\frac{E_n - 2\sqrt{E_n E_i/A_i}\cos\theta_i + E_i/A_i}{T_i}\right], \tag{2}$$

where E_n is the neutron energy in the laboratory frame, ν_i, A_i, E_i, and T_i are multiplicity, mass, kinetic energy, and temperature, respectively, of each neutron emitter. θ_i is the angle between the direction of the emitted neutron and its source. The kinetic energy of the fission fragments E_{FF} were obtained from the Viola systematics [35] assuming symmetric fission of the CN. Fission fragment folding angles were calculated assuming full momentum transfer. Angles between the emitted neutrons and their sources were determined from the scalar product of the unit vectors along neutron direction and the source (CN or fission fragment).

In this work, we have chosen the neutron energy spectra between 1 MeV and 8 MeV for the spectrum deconvolution which undoubtedly exclude contributions from pre-equilibrium emissions due to relatively higher energy of the neutrons [36]. In order to estimate the neutron multiplicity and temperature, simultaneous fitting of 50 neutron energy spectra (after efficiency correction) obtained from the 50 detectors were done at all energy points. The fitting has been performed in two ways. In the first case, $\nu_{\rm pre}$, $\nu_{\rm post}$, $T_{\rm pre}$, and $T_{\rm post}$ were treated as free parameters. In the second case, the temperature of the CN is fixed using the expression [37]

$$T_{\rm pre} = \frac{11}{12}\sqrt{\frac{E^*}{a}}, \tag{3}$$

TABLE II. Experimentally obtained values of ν_{pre}, ν_{post}, ν_{total}, T_{pre}, and T_{post} are tabulated.

E_{lab} (MeV)	E^*_{CN} (MeV)	ν_{pre}	ν_{post}	ν_{total}	T_{pre} (MeV)	T_{post} (MeV)
152.3	44.1	2.03 ± 0.16	1.07 ± 0.05	4.17 ± 0.17	1.21 ± 0.04	0.97 ± 0.03
159.4	50.2	2.17 ± 0.13	1.15 ± 0.04	4.47 ± 0.14	1.29 ± 0.05	0.99 ± 0.03
166.4	56.2	2.49 ± 0.15	1.24 ± 0.04	4.97 ± 0.16	1.33 ± 0.06	1.01 ± 0.04
173.4	62.4	2.80 ± 0.15	1.26 ± 0.06	5.32 ± 0.17	1.37 ± 0.05	1.02 ± 0.03
179.4	67.5	3.00 ± 0.18	1.28 ± 0.08	5.56 ± 0.20	1.42 ± 0.06	1.05 ± 0.04
186.4	73.6	3.40 ± 0.27	1.29 ± 0.09	5.98 ± 0.29	1.45 ± 0.06	1.07 ± 0.05
192.4	78.8	3.64 ± 0.22	1.29 ± 0.08	6.22 ± 0.24	1.51 ± 0.06	1.09 ± 0.04

where E^* is the CN excitation energy and a is the level density parameter given by $a = \frac{A_{CN}}{9}$ MeV^{-1} [38]. The obtained neutron multiplicity values using the variable temperature method were observed to be consistent with those obtained from the fixed temperature method. Figure 4 shows a typical fit of double differential neutron multiplicity spectra and its different components for 16 detectors as an example for the best fits. The total neutron multiplicity can be written as $\nu_{tot} = \nu_{pre} + 2\nu_{post}$. The best fit values of ν_{pre}, ν_{post}, T_{pre}, and T_{post} obtained from the fitting procedure for the ^{30}Si + ^{197}Au reaction are summarized in Table II.

It is observed that the contributions to total double differential neutron multiplicity spectra from different neutron emitting sources vary significantly with the laboratory angle with respect to the beam direction. This angular dependence of neutron emission from different sources is due to the kinematic focusing effect on neutrons by the fast moving sources. Measured angular distribution of energy integrated neutron multiplicity spectra at all measured energies are shown in Fig. 5 along with the simulated values. Simulation of neutron angular distribution has been performed for 0° to 180° with respect to the beam direction on either side for zero azimuthal angles (corresponding to in-plane detectors only). It is observed that the angular distribution from each neutron emitting source has a Gaussian distribution. Contributions from fission fragments are peaking around detector mean angles while contributions from the CN peak around the beam direction, which again confirm the strong angular correlations of neutron emissions due to kinematic focusing effect.

Experimental pre-scission neutron multiplicity for the ^{30}Si + ^{197}Au reaction populating the CN ^{227}Np obtained in this work is shown in Fig. 6. The ν_{pre} values reported for the ^{229}Np [39] compound system are also shown in the same plot. The ν_{pre} value increases with increasing excitation energy of the CN. The measured ν_{pre} value for the ^{229}Np does not show any significant difference from that of ^{227}Np.

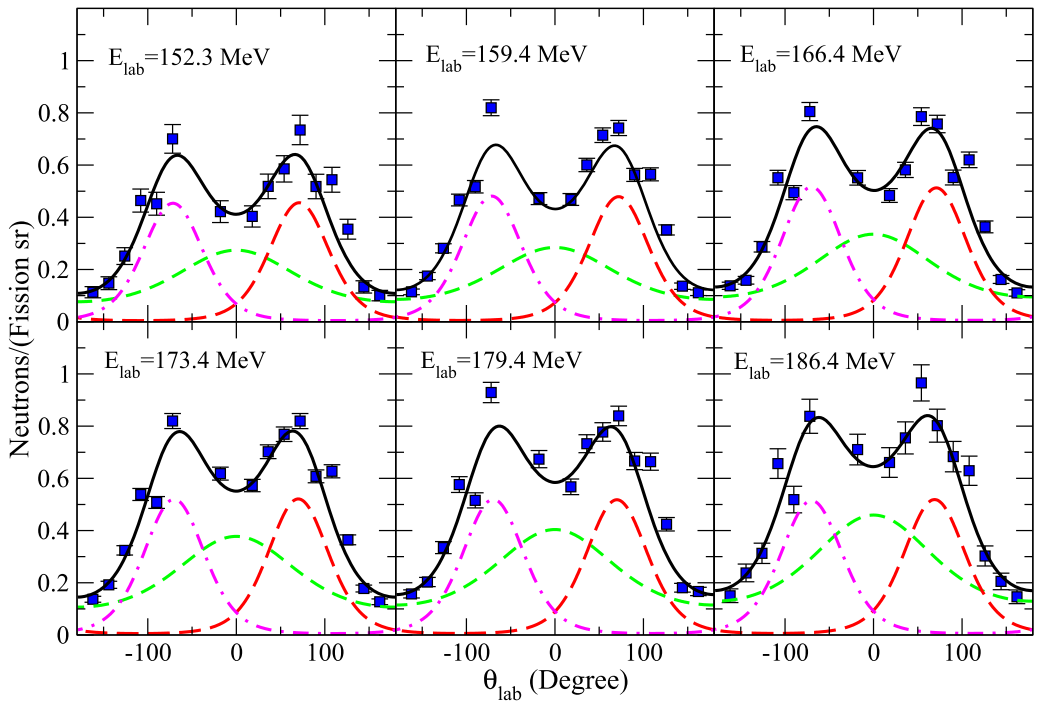

FIG. 5. Experimental neutron angular distribution (solid square) along with the simulated results (black solid line) at different energies. Angular distribution of neutrons emitted from three sources are also shown. Dashed line represents contribution from the CN, long dashed line and dot dashed line indicate the contributions from fission fragments, respectively.

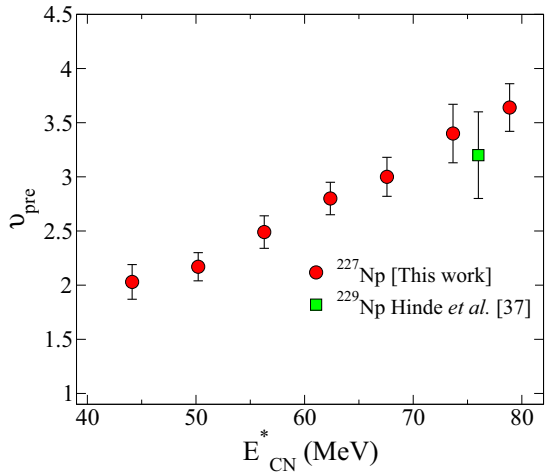

FIG. 6. Experimental ν_{pre} for ^{227}Np at different excitation energies. The ν_{pre} reported for the ^{229}Np [39] is also shown in the same plot.

IV. STATISTICAL MODEL ANALYSIS

The experimentally extracted ν_{pre} excitation function is compared with the statistical model calculations in this section. The heated CN formed in the fusion reaction decays via light particle emission, γ emission, and fission. All these decay modes are taken into account in this calculation. The fission width Γ_f is calculated from the transition-state model of fission due to Bohr and Wheeler [40] incorporating the effect of dissipation following Kramers' [3] prescription and the modification due to K degree (angular momentum component of the CN along symmetry axis) of freedom. The expression of Γ_f is given by

$$\Gamma_f(E^*, l) = \frac{\hbar\omega_g}{T}\Gamma_{BW}K_f\left\{\sqrt{1+\left(\frac{\beta}{2\omega_s}\right)^2} - \frac{\beta}{2\omega_s}\right\}, \quad (4)$$

where β denotes the reduced dissipation coefficient (ratio of dissipation coefficient to collective inertia) and ω_s (ω_g) is the frequency of the harmonic oscillator potential which approximates nuclear potential in the saddle (ground state) region and depends on the CN angular momentum (l) [41]. T represents the temperature of the CN calculated using the Fermi gas model [42]: $E^* = aT^2$; a being the level density parameter. K_f is the K-equilibration factor as described in [28,52]. Since the fission barrier for the $K \neq 0$ states is higher than the $K = 0$ state, the inclusion of K degree of freedom results in a lower fission width compared to that obtained with $K = 0$. The Γ_{BW} is calculated from

$$\Gamma_{BW}(E^*, l) = \frac{1}{2\pi\rho(E^*)}\int_0^{E^*-B_f}\rho^*(E^* - B_f - \epsilon)d\epsilon, \quad (5)$$

where the shell corrected fission barrier B_f of the CN is calculated from the angular momentum (l) dependent finite range liquid drop model (LDM) [43] fission barrier [$B_f^{\rm LDM}(l)$] as follows [44]:

$$B_f(l) = B_f^{\rm LDM}(l) - (\delta_g - \delta_s). \quad (6)$$

The shell correction energies for the ground state and saddle configurations are denoted by δ_g and δ_s, respectively. The deformation dependent shell corrections δ_g and δ_s were obtained from Ref. [45] which gives negligible shell correction at large deformations and full shell correction at zero deformation. In the expression of Γ_{BW}, ρ denotes the density of nuclear levels. It is usually constructed out of uncorrelated particle-hole states. However, correlation among the particle-hole states due to residual interaction can result in collective excitations. Inclusion of collective states can enhance the level density obtained with the independent particle model at low excitation energies. Bjørnholm, Bohr, and Mottelson [48] earlier considered the collective enhancement of level density where the collective levels are generated by adding additional degrees of freedom to those of the Fermi gas. The effective level density can thus be written as [48]

$$\rho(E^*) = K_{\rm coll}(E^*)\rho_{\rm intr}(E^*), \quad (7)$$

where $\rho_{\rm intr}(E^*)$ is the intrinsic density of states [42] and $K_{\rm coll}(E^*)$ is the factor responsible for collective enhancement in level density (CELD). The enhancement factors for collective rotation and vibration were obtained from Ignatyuk *et al.* [49]. A smooth transition from vibrational to rotational enhancement with increasing deformation was obtained by Zagrebaev *et al.* [50]. The above enhancement factor which also includes the effect of damping of collective motion with increasing excitation [51] is used in the present work.

The particle and GDR γ emission widths are obtained from the Weisskopf estimates [26]. The effect of CELD and the effect due to K-orientation are considered in calculating various decay widths. We use the level density parameter a from the work of Ignatyuk *et al.* [46],

$$a(E^*) = \tilde{a}\left(1 + \frac{f(E^*)}{E^*}\delta_g\right) \quad (8)$$

with

$$f(E^*) = 1 - \exp(-E^*/E_D), \quad (9)$$

which includes the shell effect at low excitation energies and goes over to its asymptotic value $\tilde{a}$ at higher excitation energies. The shape-dependent $\tilde{a}$ parameter given in Ref. [47] is used in the present work. The value of the damping term E_D is taken from Ref. [47].

The angular momentum of a CN though initially oriented along the perpendicular direction to the reaction plane and the symmetry axis, can subsequently change its direction due to perturbation by nuclear intrinsic motion. Thus, the angular momentum component along the symmetry axis (K) increases from zero and reaches an equilibrium distribution in course of the reaction [52].

The fission width in a stochastic dynamical model reaches its stationary value [Eq. (10)] after the elapse of a time interval. We here use the following parametrized form of time-dependent fission width [53]:

$$\Gamma_f(t) = \Gamma_K\left\{1 - e^{-\frac{2.3t}{\tau_f}}\right\}, \quad (10)$$

where τ_f is the transient time period.

In the statistical model of CN decay, fission occurs when the CN crosses the saddle point deformation. The number of neutrons emitted prior to fission as obtained in a statistical model calculation by considering competition among various decay channels therefore refers to those neutrons emitted until the CN reaches the saddle point deformation. However, further neutron emission by the CN can take place during its transition from the saddle to the scission configuration. The experimentally determined pre-scission neutron multiplicity includes all the neutrons emitted during pre-saddle and post-saddle stages until the CN splits into two fission fragments. We calculate the number of neutrons during the saddle to scission transition of a CN using the saddle-to-scission time interval which is given as [54]

$$\tau_{ss} = \tau_{ss}^{0}\left\{\sqrt{1+\left(\frac{\beta}{2\omega_s}\right)^2}+\frac{\beta}{2\omega_s}\right\}, \qquad (11)$$

where τ_{ss}^{0} is the saddle-to-scission transit time without any dissipation [54,55].

Statistical model calculations are carried out including all the features as discussed above for the reaction under study. Figure 7 shows the calculated pre-scission neutron multiplicity ($\nu_{\rm pre}$) excitation functions along with the experimental results. Statistical model predictions with the Bohr-Wheeler fission width ($\beta = 0$ zs^{-1}) are found to underestimate the pre-scission neutron multiplicity considerably as shown in Fig. 7(a). With an increase in the strength of dissipation, the calculated $\nu_{\rm pre}$ excitation function moves closer to the experimental value and a reasonable fit is obtained with $\beta =$ 10 zs^{-1}. The calculated neutron multiplicities in the saddle-to-scission ($\nu_{\rm sad\text{-}sciss}$) and pre-saddle stages ($\nu_{\rm pre\text{-}sad}$) are shown in Figs. 7(b) and 7(c), respectively. While the saddle-to-scission multiplicity is found to increase with increasing excitation energy (E^*_{CN}), the pre-saddle multiplicity remains practically stationary. Both, however, increase with increase of dissipation strength as expected.

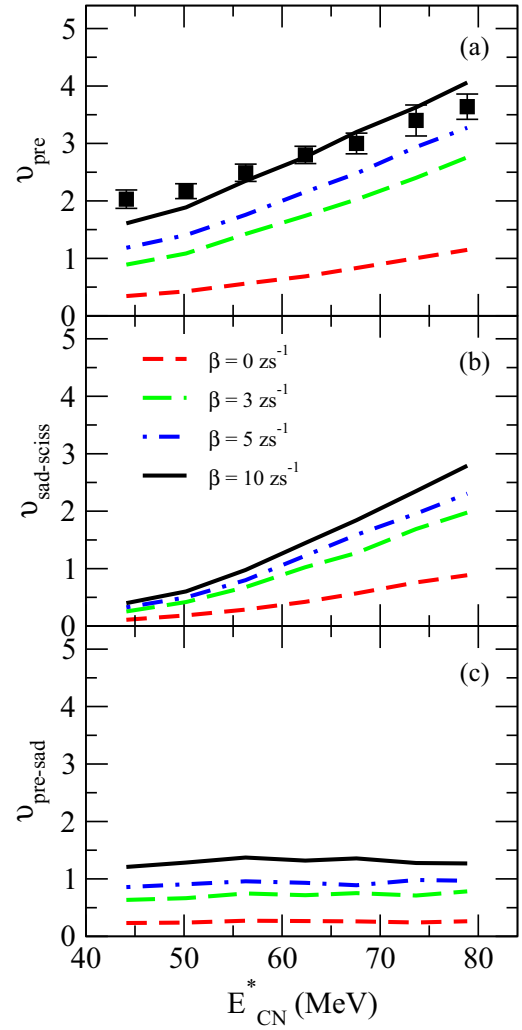

FIG. 7. Variation of $\nu_{\rm pre}$ for the ^{30}Si + ^{197}Au reaction for different dissipation strength considering the CELD and K-orientation effect in the statistical model calculations is shown in panel (a). Solid squares represent the experimental $\nu_{\rm pre}$ for the same system. Similar estimates of $\nu_{\rm sad\text{-}sciss}$ and $\nu_{\rm pre\text{-}sad}$ for different β values are also shown in (b) and (c), respectively.

V. DISCUSSION

The E^* dependence of pre-saddle and saddle-to-scission multiplicities can be qualitatively understood as follows. ^{227}Np is a highly fissile nucleus with a spin-zero LDM fission barrier of 3.7 MeV. Being highly fissile, the ER formation probability is negligibly small in this reaction in the energy range of the present study. Almost all the CN formed at excitation energies considered in the present study end up in fission. With increasing l of the CN, the ground state and the saddle shapes become closer and the LDM barrier becomes a fraction of a MeV at $l \simeq 50\hbar$. It may be pointed out here that when the LDM barrier vanishes at high angular momentum, the shell correction to the fission barrier also vanishes [Eq. (6)]. For the above reaction, the maximum angular momentum ($l_{\rm max}$) that can be imparted to the CN to reach an E^* of 50.2 MeV is $50\hbar$. Therefore, among all the CN populated with $E^* \geqslant 50$ MeV, those with $l \geqslant 50\hbar$ will have vanishingly small fission barriers with no pre-saddle stage but only saddle-to-scission transitions. Though with increasing beam energy, the fraction of compound nuclei with $l \leqslant 50\hbar$ decreases, the neutron emission probability increases. The later quantity is approximately given as $\frac{\Gamma_n}{\Gamma_f} \simeq \exp^{-(B_n-B_f)/T}$, where Γ_n and Γ_f are the neutron and fission decay widths, B_n and B_f are the neutron binding energy and fission barrier, respectively, and T is the nuclear temperature. Since $B_n > B_f$ for ^{227}Np, the above ratio and hence the neutron emission probability increases with T. Therefore the two aforementioned effects tend to cancel each other resulting in the pre-saddle contribution to $\nu_{\rm pre}$ practically independent of E^* in the energy range considered. On the other hand, the fraction of CN emitting neutrons solely in the saddle-to-scission stage increases with E^*. Therefore, the average saddle-to-scission contribution to $\nu_{\rm pre}$ also increases with E^*.

Several time scales are important in determining the pre-saddle ($\nu_{\rm pre\text{-}sad}$) and saddle-to-scission ($\nu_{\rm sad\text{-}sciss}$) contributions to $\nu_{\rm pre}$. They are the transient time period τ_f, the saddle-to-

scission transit time τ_{ss}, and the stationary fission time scale τ_{stat} given as $\hbar/\Gamma_K$. In the stochastic dynamical model of fission [52], the fission width decreases or τ_{stat} increases with increasing dissipation strength β [Eq. (4)] and thereby causing an increase of $\nu_{\text{pre-sad}}$ with increasing β. The neutron emission in the pre-saddle stage is further enhanced since the fission probability is initially suppressed over a time period of the order of the transient time τ_f [Eq. (10)] which also increases with dissipation strength [52]. Therefore, $\nu_{\text{pre-sad}}$ increases with β on account of both τ_{stat} and τ_f as found in Fig. 7(c). Both τ_{stat} and τ_f values depend on the compound nuclear spin l and excitation energy E^* and typical values for ^{227}Np at $E^* = 50$ MeV are $\tau_{\text{stat}} = 66$ zs, $\tau_f = 15$ zs for $l = 20\hbar$ and $\tau_{\text{stat}} = 32$ zs, $\tau_f = 11$ zs for $l = 40\hbar$ when a dissipation strength of $\beta = 10$ zs^{-1} is used.

The neutron multiplicity $\nu_{\text{sad-sciss}}$, on the other hand, depends solely on the saddle-to-scission transit time τ_{ss}. This transit time increases with dissipation strength [Eq. (11)] and also depends on the spin and excitation energy of the compound nucleus [53]. $\nu_{\text{sad-sciss}}$ therefore increases with an increase in the strength of dissipation coefficient as shown in Fig. 7(b). The saddle-to-scission transit time for ^{227}Np at $E^* = 50$ MeV is 20 zs for $l = 20\hbar$ and $\beta = 10$ zs^{-1} whereas it assumes a larger value at higher excitation energies and spin, e.g., $\tau_{ss} = 80$ zs at $E^* = 70$ MeV and $l = 60\hbar$. Most of the pre-scission neutrons are emitted in the above time scale at high excitation energies as has been mentioned in the previous paragraph.

It is also observed in Fig. 7 that a substantial contribution to ν_{pre} comes from the post-saddle stage. For example, the saddle-to-scission contribution increases from about 25% to 70% of the total ν_{pre} as E^* increases from 44 MeV to 79 MeV for the best-fit calculated excitation functions with $\beta = 10$ zs^{-1}. Dissipation strengths of comparable magnitudes for post-saddle shapes have also been noted in earlier works [26,27]. We next investigate the roles of CELD and K-orientation in pre-scission neutron emission. To this end, we perform three sets of calculations, one excluding CELD but keeping all other effects (i.e., K-orientation plus shell in both fission barrier and level density parameter), another excluding K-orientation but keeping others (i.e., CELD plus shell in both fission barrier and level density parameter), and the last one excluding both CELD and K-orientation but with the rest of the effects (i.e., shell in both fission barrier and level density parameter). The results are shown in Fig. 8. It is observed in Fig. 8(a) that the ν_{pre} values obtained without CELD and K-orientation effects are very close to the results of the full calculation where all the effects are included. It is also observed that ν_{pre} increases marginally with respect to those obtained in the full calculation when only CELD is excluded while it slightly decreases when only K-orientation effect is withdrawn. Both of the above trends are qualitatively expected since fission probability decreases without CELD while it increases when the K-orientation effect is excluded.

It should be mentioned at this point that while the K-orientation effect impacts only the fission width, CELD affects all the decay widths though it is the strongest for the fission channel. This is because the fission width depends on

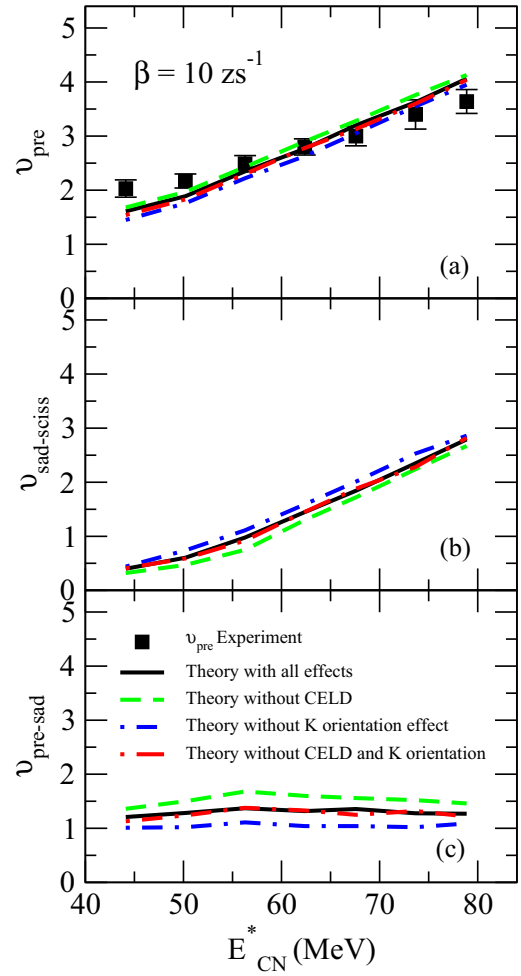

FIG. 8. Influence of CELD and K-orientation effect in ν_{pre}, $\nu_{\text{sad-sciss}}$, and $\nu_{\text{pre-sad}}$ for the ^{30}Si + ^{197}Au reaction for $\beta = 10$ zs^{-1} is demonstrated in (a), (b), and (c).

the ratio of the collective enhancement factors of the saddle and the ground state and the enhancement factor for the highly deformed saddle shape is appreciably larger than that for the more compact ground state. Since the pre-saddle timescale is determined by the fission width, the effects of K-orientation and CELD are more prominent in the pre-saddle component of ν_{pre} as is evident in Fig. 8(c). Interestingly, the saddle-to-scission contribution also shows dependence on CELD and K-orientation effects as given in Fig. 8(b) though fission width has no direct role to play in deciding the time scale of saddle-to-scission transition. Further, this dependence in the saddle-to-scission stage is smaller in magnitude but in opposite sense to that for pre-saddle neutrons, e.g., saddle-to-scission contribution to ν_{pre} decreases without CELD whereas the pre-saddle multiplicity increases and vice versa for the K-orientation effect. The above dependence in the saddle-to-scission stage is a consequence of the effects in the pre-saddle stage. If the number of pre-saddle neutrons increases, the excitation energy available in the saddle-to-scission stage decreases and consequently the saddle-to-scission contribution to ν_{pre} also decreases.

It may further be noted that the CELD and K-orientation effects depend on the system concerned and the small effect observed here is specific to the reaction considered in the present study. The large deformation of the ^{227}Np nucleus in its ground state (the quadrupole deformation parameter is 0.153 [56]) gives rise to a higher collective enhancement factor than that for the spherical shape. The fission width depends on the ratio of the collective enhancement factors of the saddle and the ground state and consequently the effect of CELD is weaker for the fission width of a deformed nucleus than that for a spherical one. The K-orientation effect, on the other hand, increases with the spin of the CN [52]. However, as we have noticed earlier, the maximum spin of the ^{227}Np CN which faces a fission barrier is about $50\hbar$ and, therefore, the K-orientation effect is also limited to CN carrying spin of the above value.

Though we find in the present study that $\nu_{\rm pre}$ is not a sensitive tool to explore effects such as CELD for the highly fissile CN ^{227}Np, it may not be so for the ER cross section. When fission cross section is larger than the ER cross section, a small change in the fission width changes the fission cross section only by a smaller fraction than the corresponding fractional change in the ER cross section. Therefore, ER cross section is expected to be a more sensitive probe for the fission process for reactions with small ER cross sections (such as nuclei in the actinide region). In this context, it may be pointed out that CELD was found necessary to reproduce ER production cross sections of ^{45}Sc induced reactions on lanthanide targets [30]. More systematic work is necessary for a better understanding of the roles of various factors contributing to fission of hot rotating nuclei.

VI. SUMMARY AND CONCLUSION

Neutron multiplicities have been measured for the ^{30}Si + ^{197}Au reaction populating the ^{227}Np CN over a wide range of excitation energies using the NAND facility. The measured $\nu_{\rm pre}$ data were analyzed within the framework of a statistical model including the effect of CELD, K-orientation effect, and dissipation in fission dynamics. Measurement of $\nu_{\rm pre}$ for such a heavy fissile system explicitly provides direct evidence for the presence of a strong nuclear dissipation hindering the fission of hot and rapidly rotating CN. The emission of neutrons at higher excitation energies (or larger angular momentum results in vanishing of fission barrier) could only be understood in terms of nuclear dissipation. Energy dependence of nuclear dissipation could not be observed as reported in a few recent $\nu_{\rm pre}$ measurements. Analyses show that the emission of saddle-to-scission neutrons which increase with excitation energy of the CN contribute more to the $\nu_{\rm pre}$ than pre-saddle neutron emission. However, the $\nu_{\rm pre\text{-}sad}$ for ^{227}Np CN does not show dependence on excitation energy. Influence of CELD and K-orientation degrees of freedom in fission of such heavy nuclei are observed to be small unlike the fission of preactinides, which could be attributed to the large deformation at the ground state of the CN and the limit to populate maximum angular momentum in the CN, respectively. More experimental and theoretical studies are warranted in the actinide region in order to better understand the aforementioned effects.

ACKNOWLEDGMENTS

The authors gratefully acknowledge the Pelletron and LINAC crew of IUAC, New Delhi for providing excellent quality beam throughout the experiment. Two of the authors (M.S. and A.C.V.) acknowledge Kerala State Council for Science Technology and Environment (KSCSTE) for financial aid. One of the authors (E.P.) acknowledges DST for providing support in the form of a DST-RFBR fellowship. We acknowledge the DST, Government of India for NAND project under Grant. No. IR/S2/PF-02/2007.

[1] A. N. Andreyev, K. Nishio, and K.-H. Schmidt, Rep. Prog. Phys. **81**, 016301 (2018).
[2] P. Grange and H. A. Weidenmuller, Phys. Lett. B **96**, 26 (1980).
[3] H. A. Kramers, Physica **7**, 284 (1940).
[4] B. B. Back, D. J. Blumenthal, C. N. Davids, D. J. Henderson, R. Hermann, D. J. Hofman, C. L. Jiang, H. T. Penttilä, and A. H. Wuosmaa, Phys. Rev. C **60**, 044602 (1999).
[5] Varinderjit Singh, B. R. Behera, Maninder Kaur, A. Kumar, P. Sugathan, K. S. Golda, A. Jhingan, M. B. Chatterjee, R. K. Bhowmik, Davinder Siwal, S. Goyal, Jhilam Sadhukhan, Santanu Pal, A. Saxena, S. Santra, and S. Kailas, Phys. Rev. C **87**, 064601 (2013).
[6] E. Prasad, K. M. Varier, N. Madhavan, S. Nath, J. Gehlot, Sunil Kalkal, Jhilam Sadhukhan, G. Mohanto, P. Sugathan, A. Jhingan, B. R. S. Babu, T. Varughese, K. S. Golda, B. P. Ajith Kumar, B. Satheesh, Santanu Pal, R. Singh, A. K. Sinha, and S. Kailas, Phys. Rev. C **84**, 064606 (2011).
[7] D. J. Hinde, M. Dasgupta, J. R. Leigh, J. P. Lestone, J. C. Mein, C. R. Morton, J. O. Newton, and H. Timmers, Phys. Rev. Lett. **74**, 1295 (1995).
[8] B. B. Back, P. B. Fernandez, B. G. Glagola, D. Henderson, S. Kaufman, J. G. Keller, S. J. Sanders, F. Videbæk, T. F. Wang, and B. D. Wilkins, Phys. Rev. C **53**, 1734 (1996).
[9] Y. Aritomo, M. Ohta, T. Materna, F. Hanappe, O. Dorvaux, and L. Stuttge, Nucl. Phys. A **759**, 309 (2005).
[10] P. Fröbrich and H. Rossner, Z. Phys. A **349**, 99 (1994).
[11] P. N. Nadtochy, G. D. Adeev, and A. V. Karpov, Phys. Rev. C **65**, 064615 (2002).
[12] D. Hilscher and H. Rossner, Ann. Phys. Fr. **17**, 471 (1992).
[13] D. J. Hinde, R. J. Charity, G. S. Foote, J. R. Leigh, J. O. Newton, S. Ogaza, and A. Chatterjee, Nucl. Phys. A **452**, 550 (1986).
[14] J. O. Newton, D. J. Hinde, R. J. Charity, J. R. Leigh, J. J. M. Bokhorst, A. Chatterjee, G. S. Foote, and S. Ogaza, Nucl. Phys. A **483**, 126 (1988).
[15] R. Sandal, B. R. Behera, Varinderjit Singh, Maninder Kaur, A. Kumar, G. Singh, K. P. Singh, P. Sugathan, A. Jhingan, K. S. Golda, M. B. Chatterjee, R. K. Bhowmik, Sunil Kalkal, D. Siwal, S. Goyal, S. Mandal, E. Prasad, K. Mahata, A. Saxena, J. Sadhukhan, and S. Pal, Phys. Rev. C **87**, 014604 (2013).

[16] M. Shareef, A. Chatterjee, and E. Prasad, Eur. Phys. J. A **52**, 342 (2016).
[17] H. Ikezoe, N. Shikazono, Y. Nagame, Y. Sugiyama, Y. Tomita, K. Ideno, I. Nishinaka, B. J. Qi, H. J. Kim, A. Iwamoto, and T. Ohtsuki, Phys. Rev. C **46**, 1922 (1992).
[18] J. P. Lestone, J. R. Leigh, J. O. Newton, D. J. Hinde, J. X. Wei, J. X. Chen, S. E. Elfstrom, and D. G. Popescu, Phys. Rev. Lett. **67**, 1078 (1991).
[19] A. Chatterjee, A. Navin, S. Kailas, P. Singh, D. C. Biswas, A. Karnik, and S. S. Kapoor, Phys. Rev. C **52**, 3167 (1995).
[20] P. Paul and M. Thoennessen, Annu. Rev. Nucl. Part. Sci. **44**, 65 (1994).
[21] D. J. Hofman, B. B. Back, I. Dioszegi, C. P. Montoya, S. Schadmand, R. Varma, and P. Paul, Phys. Rev. Lett. **72**, 470 (1994).
[22] M. Thoennessen, D. R. Chakrabarty, M. G. Herman, R. Butsch, and P. Paul, Phys. Rev. Lett. **59**, 2860 (1987).
[23] A. Gavron, J. R. Beene, B. Cheynis, R. L. Ferguson, F. E. Obenshain, F. Plasil, G. R. Young, G. A. Petitt, M. Jääskeläinen, D. G. Sarantites, and C. F. Maguire, Phys. Rev. Lett. **47**, 1255 (1981).
[24] D. Jacquet and M. Morjean, Prog. Part. Nucl. Phys. **63**, 155 (2009).
[25] I. Diószegi, N. P. Shaw, I. Mazumdar, A. Hatzikoutelis, and P. Paul, Phys. Rev. C **61**, 024613 (2000).
[26] P. Fröbrich and I. I. Gontchar, Phys. Rep. **292**, 131 (1998).
[27] G. Chaudhuri and S. Pal, Phys. Rev. C **63**, 064603 (2001).
[28] T. Banerjee, S. Nath, and Santanu Pal, Phys. Lett. B **776**, 163 (2018).
[29] K. Siwek-Wilczyńska, I. Skwira, and J. Wilczyński, Phys. Rev. C **72**, 034605 (2005).
[30] T. A. Werke, D. A. Mayorov, M. C. Alfonso, M. E. Bennett, M. J. DeVanzo, M. M. Frey, E. E. Tereshatov, and C. M. Folden III, Phys. Rev. C **92**, 034613 (2015).
[31] P. Sugathan, A. Jhingan, K. S. Golda, T. Varughese, S. Venkataraman, N. Saneesh, V. V. Satyanarayana, S. K. Suman, J. Antony, R. Shanti, K. Singh, S. K. Saini, A. Gupta, A. Kothari, P. Barua, Rajesh Kumar, J. Zacharias, R. P. Singh, B. R. Behera, S. K. Mandal, I. M. Govil, and R. K. Bhowmik, Pramana **83**, 807 (2014).
[32] S. Venkataramanan, Arti Gupta, K. S. Golda, Hardev Singh, Rakesh Kumar, R. P. Singh, and R. K. Bhowmik, Nucl. Instrum. Methods Phys. Res. A **596**, 248 (2008).
[33] http://www.tifr.res.in/-pl2X-sim-pell/lamps.html.
[34] D. Hilscher, J. R. Birkelund, A. D. Hoover, W. U. Schröder, W. W. Wilcke, J. R. Huizenga, A. C. Mignerey, K. L. Wolf, H. F. Breuer, and V. E. Viola, Phys. Rev. C **20**, 576 (1979).
[35] V. E. Viola, K. Kwiatkowski, and M. Walker, Phys. Rev. C **31**, 1550 (1985).
[36] V. A. Rubchenya, A. V. Kuznetsov, W. H. Trzaska, D. N. Vakhtin, A. A. Alexandrov, I. D. Alkhazov, J. Äystö, S. V. Khlebnikov, V. G. Lyapin, O. I. Osetrov, Yu. E. Penionzhkevich, Yu. V. Pyatkov, and G. P. Tiourin, Phys. Rev. C **58**, 1587 (1998).
[37] E. Holub, D. Hilscher, G. Ingold, U. Jahnke, H. Orf, and H. Rossner, Phys. Rev. C **28**, 252 (1983).
[38] K. S. Golda, A. Saxena, V. K. Mittal, K. Mahata, P. Sugathan, A. Jhingan, V. Singh, R. Sandal, S. Goyal, J. Gehlot, A. Dhal, B. R. Behera, R. K. Bhowmik, and S. Kailas, Nucl. Phys. A **913**, 157 (2013).
[39] D. J. Hinde, H. Ogata, M. Tanaka, T. Shimoda, N. Takahashi, A. Shinohara, S. Wakamatsu, K. Katori, and H. Okamura, Phys. Rev. C **39**, 2268 (1989).
[40] N. Bohr and J. A. Wheeler, Phys. Rev. **56**, 426 (1939).
[41] J. Sadhukhan and S. Pal, Phys. Rev. C **78**, 011603(R) (2008).
[42] A. Bohr and B. R. Mottelson, *Nuclear Structure*, Vol. 1 (Benjamin Press, New York, 1969).
[43] A. J. Sierk, Phys. Rev. C **33**, 2039 (1986).
[44] K. Mahata, S. Kailas, and S. S. Kapoor, Phys. Rev. C **92**, 034602 (2015).
[45] W. D. Myers and W. J. Swiatecki, Nucl. Phys. **81**, 1 (1966).
[46] A. V. Ignatyuk, M. G. Itkis, V. N. Okolovich, G. M. Smirenkin and A. Tishin, Yad. Fiz. **21**, 485 (1975) [Sov. J. Nucl. Phys. **21**, 255 (1975)].
[47] W. Reisdorf, Z. Phys. A **300**, 227 (1981).
[48] S. Bjørnholm, A. Bohr, and B. R. Mottelson, *Proceedings of the International Conference on the Physics and Chemistry of Fission*, Vol. 1, Rochester, NY, 1973 (IAEA, Vienna, 1974), p. 367.
[49] A. V. Ignatyuk, G. N. Smirenkin, M. G. Itkis, S. I. Mulgin, and V. N. Okolovich, Sov. J. Part. Nucl. **16**, 307 (1985).
[50] V. I. Zagrebaev, Y. Aritomo, M. G. Itkis, Yu. T. Oganessian, and M. Ohta, Phys. Rev. C **65**, 014607 (2001).
[51] A. R. Junghans, M. de Jong, H.-G. Clerc, A. V. Ignatyuk, G. A. Kudyaev, and K.-H. Schmidt, Nucl. Phys. A **629**, 635 (1998).
[52] J. P. Lestone, Phys. Rev. C **59**, 1540 (1999).
[53] K. H. Bhatt, P. Grangé, and B. Hiller, Phys. Rev. C **33**, 954 (1986).
[54] H. Hofmann and J. R. Nix, Phys. Lett. B **122**, 117 (1983).
[55] P. Grangé, S. Hassani, H. A. Weidenmüller, A. Gavron, J. R. Nix, and A. J. Sierk, Phys. Rev. C **34**, 209 (1986).
[56] P. Möller, A. J. Sierk, T. Ichikawa, and H. Sagawa, At. Data Nucl. Data Tables **109–110**, 1 (2016).